



**HAL**  
open science

# Effect of NbC Addition on the High-Temperature Oxidation Resistance of Co- and Ni-Based Chromium-Rich Alloys

Mélissa Ritouet, Patrice Berthod

► **To cite this version:**

Mélissa Ritouet, Patrice Berthod. Effect of NbC Addition on the High-Temperature Oxidation Resistance of Co- and Ni-Based Chromium-Rich Alloys. *Oxidation of Metals*, 2018, 89 (3-4), pp.339-355. 10.1007/s11085-017-9790-9 . hal-02181316

**HAL Id: hal-02181316**

**<https://hal.science/hal-02181316>**

Submitted on 12 Jul 2019

**HAL** is a multi-disciplinary open access archive for the deposit and dissemination of scientific research documents, whether they are published or not. The documents may come from teaching and research institutions in France or abroad, or from public or private research centers.

L'archive ouverte pluridisciplinaire **HAL**, est destinée au dépôt et à la diffusion de documents scientifiques de niveau recherche, publiés ou non, émanant des établissements d'enseignement et de recherche français ou étrangers, des laboratoires publics ou privés.

# Effect of NbC Addition on the High Temperature Oxidation Resistance of Co- and Ni-base Chromium-rich Alloys

Mélissa Ritouet, Patrice Berthod

*Institut Jean Lamour (UMR CNRS 7198), Department CP2S, Faculty of Science and Technologies, Postal Box 70239, 54506 Vandoeuvre-lès-Nancy, FRANCE*

[melissa.ritouet@univ-lorraine.fr](mailto:melissa.ritouet@univ-lorraine.fr), [patrice.berthod@centraliens-lille.org](mailto:patrice.berthod@centraliens-lille.org)

**Abstract.** Two {M-25Cr}-based alloys, with M=Co or Ni, containing 0.5C and 3.9Nb (wt.%) to favor the crystallization of NbC carbides during solidification were elaborated by casting and subjected to oxidation in air at 1000, 1100 and 1200°C for 46 hours. The results were studied by comparison with recent similar ones obtained with Nb-free ternary alloys issued from the same elaboration protocol and tested in oxidation in the same conditions. In both cases interdendritic script-like shaped NbC carbides were obtained as expected, however not as single carbides in the nickel alloy which also contain chromium carbides. Preliminary exposure to 1200°C having shown a morphological evolution of the NbC, as-cast and preliminarily aged versions of both alloys were tested in oxidation. It appeared first that, whatever the aged state, the cobalt alloy behaved much worse than the nickel one, that the presence of Nb deteriorated the behavior in both cases but at a much lower scale and that aging alloys, which results in NbC fragmentation, was also detrimental for the high temperature oxidation behavior.

**Keywords:** Cobalt-based alloys; Nickel-based alloys; Niobium carbides; High temperature oxidation; Mass gain rates; Scale spallation; Oxide characteristics

Post-print version of the article *Oxid Met* (2018) 89:339–355; <https://doi.org/10.1007/s11085-017-9790-9>

## INTRODUCTION

Increasing service temperature to enhance both performance and efficiency creates a demand of new alloys superior to the best present superalloys, the single crystalline  $\gamma/\gamma'$  nickel-based ones [1]. Candidates are cobalt-based particularly rich in heavy elements [2] or containing  $\gamma'$  precipitates [3], refractory High Entropy Alloys (HEA) [4], for instance. Another possible way consists in revisiting rather old metallurgical principles as cobalt-based and nickel-based carbide-strengthened chromia-forming by replacing the usual chromium or tantalum carbides by new hardening particles [5]. This was recently done with conventionally cast chromium-rich cobalt-based [6], iron-based [7] and nickel-based [8] alloys strengthened by eutectic HfC carbides. These new model alloys displayed interesting mechanical properties at temperatures as high as 1100°C [9] and even 1200°C [10]. Beside TaC and HfC, other MC carbides may be considered, involving metals not so expensive as tantalum and hafnium in particular. Many of them may crystallize with a mechanically favorable script-like morphology, as demonstrated with recently investigated polycrystalline cobalt-based [11] and nickel-based [12] alloys, with consequently potential creep resistance at very high temperature (e.g. 1200°C). NbC is one of these MC carbides crystallizing with a script-like shape forming an interdendritic eutectic compound in which it is imbricated with the periphery of the solidification dendrites. Niobium is already wellknown in the superalloys' world since it is used as a  $\gamma'$ -former element beside Al and it can be even employed as base element in some refractory metallic alloys [13,14]. In contrast, although the presence of NbC carbides was previously reported several times in literature, it seems that increasing the high temperature creep resistance of superalloys by exploiting NbC carbides as single strengthening particles was not envisaged. This is the reason why one undertook the exploration of the microstructures and high temperature properties of cast cobalt-based and nickel-based polycrystalline model alloys, containing Nb and C in quantities allowing obtaining sufficiently high density of NbC carbides (0.5C and 3.9Nb, in wt.%), as well as high chromium content (25wt.%) of

the same level as many chromia-forming superalloys [15]. In parallel to the ongoing mechanical characterization at high temperature, the high temperature oxidation behavior of these alloys was studied.

These are the results of these investigations specifically concerning hot oxidation which are presented in this work, thus for two conventionally cast alloys, a Co-25Cr-0.5C-3.9Nb one and a Ni-25Cr-0.5C-3.9Nb one. In order to enlarge the characterization, by examining the behavior of a new alloy and the one of a already used one, the investigations concerned two distinct versions of these alloys: a as-cast one and a preliminarily aged one.

## EXPERIMENTAL

The compositions of the elaborated alloys, named CoNb and NiNb, are given in Table 1. These alloys contain 25% of chromium (to favor a chromia-forming behavior) and the same molar quantity of C and Nb to promote the formation of MC type carbides. The alloys were elaborated from solids parts of pure elements (purity >99.9%) under argon. These ones were synthesized in a high frequency induction furnace (CELES, France), with melting and solidification achieved in water-cooled copper crucible. The obtained ingots weighed about 40g. These ingots were cut in two equivalent parts using a Delta Abrasimet saw (Buehler). The first part was studied in its as-cast state and the second part had undergone a heat treatment in order to simulate an aging in service. This dwell at high temperature was carried out in a tubular furnace, at 1200°C during 100h. The ingots were placed in the oven at the room temperature and the heating rate was of 20°C/min. After 100h at high temperature, the alloys were extracted from the furnace and they were cooled in room air. The aged versions of the NiNb and CoNb alloy were named NiNbR and CoNbR respectively. All the half-ingots were cut with Secotom 50 microsaw (Struers) to obtain the samples for the oxidation tests: their dimensions were  $6 \times 6 \times 2 \text{ mm}^3$ . Then, these samples were polished with SiC papers from #400 to #1200 by rounding the edges to avoid local over oxidation and too high growth stresses in the oxide scales. A Setaram TG92 thermobalance (Setaram) was used for the thermogravimetry tests which were performed at 1000°C, 1100°C and 1200°C during 46h. The samples were suspended in chamber through which synthetic dry air (80% of N<sub>2</sub> and 20% of O<sub>2</sub>) circulated (flow rate of 1.5L/hour). After the oxidation tests, the specimens were cut in two halves. The halves were embedded in CY230 resin mix with a HY956 hardener (Escil). The embedded samples were polished with SiC papers from #400 to #4000 then with a synthetic velor drape enriched with a solution containing alumina particles of 0.02 μm in diameter to have mirror-like state. And to finish, they were ultrasonically cleaned with ethanol. SEM images in back-scattered electrons (BSE) mode, EDS and XRD analyses were carried out on these samples in order to observe and to define their microstructures, the sub-surfaces state and the oxides formed. A JSM-6010LA (Jeol) electronic microscope equipped with an EDS analyzer was used. The images and the analyses were made with an acceleration voltage of 20kV. The X-ray diffractions were realized with a X'Pert Pro (Philips) diffractometer using a Bragg-Brentano (θ-2θ) assembly. The X-rays source was a copper anti-cathode (Kα1, λ=1.54056 Å). The indexation of the obtained diffractograms was performed with a Diffrac AT software using the EVA module working with the PDF2 database.

## RESULTS

### The microstructures of both alloys in their as-cast and preliminarily aged states

The microstructures of the two alloys before and after the heat treatment are showed in Figure 1. NbC and chromium carbides have precipitated during solidification in the NiNb alloy, while in the CoNb alloy, only NbC carbides are present. These carbides are located in the interdendritic spaces and have a script-like shape. After heat treatment, niobium and chromium carbides have adopted a more circular shape; they get fragmented in order to reduce their matrix/carbide interfacial energy, a classical phenomenon. The obtained microstructures can be compared to the ones of as-cast ternary alloys earlier studied: Ni-25Cr-0.5 [9] and Co-25Cr-0.5C [16] (in wt.%), which can play the role of Nb-free references. In these ternary alloys, only chromium carbides were present. The chromium carbide population in the NiNb alloy is less important than in the corresponding reference alloy. In the CoNb alloy there are some chromium carbides in the reference alloy (but a small quantity) whereas no chromium carbide is present in CoNb alloy. In both Nb-containing alloys Nb appeared as being a stronger carbide-former element than chromium, but more in a cobalt base than in a nickel base.

## Mass gain kinetics

Thermogravimetry tests were performed at 1000°C, 1100°C and 1200°C during 46h. The mass gain curves versus time plotted from these thermogravimetry results are showed in Figure 2. At all temperatures and for both states (as-cast or aged “R”), the mass gains are lower for the Ni-based alloy than for the Co-based one. Contrarily to the Ni-based alloys, at lower temperatures, the mass gains are not parabolic for the Co-based alloys. Previous works indicated that the mass gains after 50h for the Co-based reference alloy are approximately  $5 \times 10^{-3}$  g/cm<sup>2</sup> at 1100°C [17] and  $1.1 \times 10^{-2}$  g/cm<sup>2</sup> at 1200°C [16] and at 1100°C the mass gain curve is not parabolic. Therefore, the total mass gain for the Nb-containing cobalt alloy is greater than for the Nb-free one. Concerning the nickel alloys, according to an earlier work [1], at 1100°C, the obtained mass gain after 46h of oxidation for the Ni-25-0.5C ternary alloy is near  $1.3 \times 10^{-3}$  g/cm<sup>2</sup>. For the NiNb alloy (in this work), the mass gain after 46h is  $2.6 \times 10^{-3}$  g/cm<sup>2</sup>, which is twice the one of the reference alloy. About the aging, it appears that it has an influence on mass gain for the CoNb alloy, more precisely it is harmful. In contrast, the aging doesn't influence the mass gain for the Ni-base alloy, except at 1000°C, temperature at which the mass gain is more important after the aging.

Since the corrosion products observed over the oxidized sample are never only chromia as this will be said farther in the text, and often a complex mix of several oxides, it was not attempted to value neither mass loss by chromia volatilization nor the kinetic constant associated to this phenomenon despite this one can be expected considering the high level of at least two of the three test temperatures. The mass gain curves were thus only exploited to determine the kinetic constant  $k_p$  according to the classical equation (1):

$$(d(\Delta m))/dt = k_p / \Delta m \quad (1)$$

where  $\Delta m$  in the mass gain per surface unit area.

The  $k_p$  values are displayed in Table 2. They confirm the observations made above by comparing the obtained mass gain curves.

For the Ni-base alloy and for its two states (as-cast or preliminarily aged), the mass gain curves obey a parabolic law, at all temperatures. By looking to both curves and  $k_p$  values, one finds again that the prior aging influences the mass gain kinetic, especially at 1000°C.

For the Co-base alloy, before and after the aging, at the lowest temperatures, the mass gain curves are not parabolic. At the 1200°C (and 1100°C too for the first aged alloy), the mass gain curves seem parabolic for the CoNb and the CoNbR alloys, this allowing determining values for  $k_p$ . The obviously fast mass gains suggest that the alloys have not a chromino-forming behavior. This suggestion will be subsequently verified by the study of the formed oxides.

If compared to the data in the bibliography on ternary alloys being considered as Nb-free versions of the alloys studied in this work (see Table 3), the values obtained here for Nb-containing alloys are a little higher for the Ni-based alloy. For example the  $k_p$  value for Ni-25Cr-0.5C at 1100°C [9] is  $5.5 \times 10^{-12}$  g<sup>2</sup>.cm<sup>-4</sup>.s<sup>-1</sup>. For the Co-base alloy, there is a factor of 10 between the  $k_p$  values obtained for CoNb and the corresponding Nb-free alloy [16, 17]. The observations are the same than above with the total mass gain data.

## Oxide spallation during cooling

With the results of the thermogravimetric tests, it is possible to know the tendency to the spallation of the oxide layer during the cooling by plotting the mass gain versus the temperature. In advance, it is necessary to deduce the Archimedean buoyant force because this one is function of the temperature. These results for both alloys at all test temperatures are represented in Figure 3. Two parameters can be deduced from this representation: a temperature of spallation start and the lost mass. These data are presented in Table 4. The annealing seems to have no influence on the spallation behavior. At 1000°C, the oxide layers on Co-based alloy put up with the spallation (temperatures of spallation's are about 310°C and the lost masses are the double of the mass gains after 46h of oxidation) whereas the oxide layers on the Ni-based alloy do not spall off at this temperature. At the highest temperatures (1100°C and 1200°C), it is the contrary. There is no spallation for the CoNb and CoNbR alloys but the Ni-based alloy puts up with spallation of oxide layers with as data: spallation's start temperatures of 745°C and 865°C and masses lost during the cooling of about  $7 \times 10^{-3}$  g/cm<sup>2</sup> and  $1.7 \times 10^{-2}$  g/cm<sup>2</sup> at 1100°C and 1200°C respectively. The temperature of start's spallation seems to increase with the temperature of test. In the cases where the oxide layer spalled off, the lost mass is practically the double of mass gain during the oxidation during 46h, therefore the spallation is too important in all cases. During the thermogravimetric tests carried out by Berthod et al. of the Co-25Cr0.5C alloy at 1100°C [17] and 1200°C [16], a spallation of oxide layers was noted during the cooling but it is not the case in the

present study with the Nb-containing alloy. The addition of Nb seems to improve the adhesion of oxide layer at 1100°C and 1200°C.

To summarize, the exploitation of the cooling part of the mass variation files allowed finding that:

- the thickest the chromia scale (due to high stage temperature, or scale also containing other oxides but chromia still being the most present one), the sooner the spallation start during cooling (cases of the Ni-based alloys), and no spallation for thin scales (NiNb and NiNbR, 1000°C)
- the highest stage temperature of the Ni-based alloys, the sooner the spallation start
- spallation a little sooner for the aged Ni-based alloys than for the as-cast ones
- spallation is very late for the cobalt alloys (rather thick oxide scale) for a cooling after a 1000°C stage, while no spallation occurs after a stage at higher temperature (too thick - and then resistant enough - scales to spall off during cooling).

These observations well meet earlier ones done for more numerous alloys and reported in [18]. In addition, it appeared here that the presence of Nb seemed to be favorable for a better resistance of external oxides against spallation at cooling.

## Analysis of the external oxides

To determine the formed oxides during the oxidation, EDS spot analyses and XRD analyses were carried out on the oxides formed on the oxidized samples. The SEM/BSE images of oxide layers are showed, for oxidation temperature of 1000°C, in Figure 4, for 1100°C in Figure 5 and for 1200°C in Figure 6. For the Ni-based alloy, the NbCrO<sub>4</sub> is formed at the matrix/oxide interface, except at 1000°C for as-cast state. Above, a chromia layer is present. And at lower temperature, the outer layer of Ni and Cr spinel oxide is formed. There is too NiO which is present in addition at 1000°C for this alloy after the aging. The formed oxides in the case of the Co-base alloy are very different. For all temperatures and all states, an inner layer of chromia is detected. Then, there is a complex mixture of several oxides. It is a mixture of CoCr<sub>2</sub>O<sub>4</sub>, Nb oxide and sometimes CoO and chromia. And to finish, for a few cases, the important outer layer of CoO oxide is formed. It should be noted that, in some cases, the oxide layer has peeled, as indicated above, therefore other oxides were maybe formed but they could not be detected and visualized in these cases. As the mass gain, the aging has only a little influence on formed oxides.

The Nb-free Ni-based alloy [9] has a chromia-forming behavior at 1100°C since only the Cr<sub>2</sub>O<sub>3</sub> layer is formed hence the mass gain is low. This chromia layer protected the alloy from oxidation by acting as diffusion barrier to O and Ni, which avoided the formation of NiO and NiCr<sub>2</sub>O<sub>4</sub>. This is not the case for the Nb-containing alloy where the formation of NbCrO<sub>4</sub> had obstructed the quick formation of chromia. For the Nb-free Co-based alloy oxidized at 1100°C [17] and 1200°C [16], the appearance of oxide layer is alike the Nb-containing alloy. An outer scale of CoO is present. Below, at 1100°C for the ternary alloy, only a chromia layer is formed while for CoNb and CoNbR alloys, CoCr<sub>2</sub>O<sub>4</sub> and Nb oxide in addition of Cr<sub>2</sub>O<sub>3</sub> also are detected. And at 1200°C, below the CoO oxide layer, for the reference alloy, a Co and Cr spinel oxide scale is formed, then there is an inner mixture layer of both oxides (Cr<sub>2</sub>O<sub>3</sub> + CoCr<sub>2</sub>O<sub>4</sub>). And for Nb-containing alloy, it is almost similar with only the mix of the both oxides with in addition of Nb oxide.

## Thicknesses of the oxide scales

The SEM images of oxide layers were used to measure their thicknesses in three zones for each alloy. The averages and standard deviations of these measures are represented in Figure 7. The points which were surrounded mean that the oxide layers had spalled off during the cooling and therefore the measured thicknesses are maybe lower than the real ones. It can be observed that, as the previous results, the heat treatment has only a little influence on this parameter and its influence is random. For the Ni-based alloy, the oxide scales have spalled off at higher temperatures, thus no conclusion is possible. For the CoNb and CoNbR alloys, the oxide layers are thick especially at higher temperature, it is due at the formation of CoO and spinel oxide which are porous oxides with a lot of defaults (gaps). In regarding the SEM images of oxide layers of ternary alloy in literature, the thicknesses of the oxide scales are about 20 µm and about 320 µm for the oxidized sample at 1100°C [17] and 1200°C [16] respectively but the oxide layers have spalled for this ternary alloy. Despite the spallation, the oxide layer at 1200°C is thick because CoO and spinel oxide are also formed.

## Characterization of the subsurface affected by oxidation

EDS spot analyses were performed at sub-surfaces of samples to establish concentration profiles as seen in Figure 8. Obviously, not only a Cr-depleted zone is developed but also a NbC-free zone and a Cr<sub>23</sub>C<sub>6</sub>-free zone. The depths of these zones are measured and reported on the graphs which are showed in Figure 9. For the Ni-based alloy, the NbC-free zones are thinner than the chromium carbide-free zones. Then, two remarks can be made. Firstly, the oxidation is more important for the Co-based alloy than for the Ni-based one but all depths are higher for this last one. Secondly, as the above results, the depths of Cr-depleted zones and carbides-free zones obtained before and after the aging are a little different. These measured results before the heat treatment are little lower than these obtained ones after the aging whereas the oxidation of the aged samples was slightly higher than of as-cast samples.

The behavior of Nb in the subsurface during oxidation appears to be curious. Indeed, in contrast with chromium here (well-known phenomenon in the case of Cr), or tantalum in earlier studies (for example [5]), which both decrease in content when approaching the oxide/alloy interface, the Nb content obviously increases when coming close to the extreme surface of the alloy. This was previously noticed for a Co(bal.)-8Ni-30Cr-0.4C-3.3Nb (wt.%) alloy oxidized for 20 hours at 1300°C [5], as well as for the 625 Ni-based alloy after much longer oxidation at temperatures ranging from 700 and 1000°C [19, 20].

## DISCUSSION

Niobium introduction in well-known cobalt-chromium and nickel-chromium bases successfully led to the wished microstructure: dendritic matrix with significant interdendritic script-like NbC carbides mixed with the dendrites periphery. This is particularly true for the cobalt alloy for which all carbon was involved in NbC carbides, with furthermore keeping of this state during exposure at 1200°C for a rather long time (100 hours). This is less true for the nickel alloy in which chromium carbides co-exist with NbC. However the latter carbides are script-like shaped and it does not disappear during long exposure at elevated temperature. Unfortunately, in both cases the NbC carbide network becomes rather rapidly fragmented. Beside the detrimental effect that one can anticipate for the bulk mechanical properties at high temperature, this morphological evolution of the NbC carbides may influence the high temperature oxidation behavior of the alloys.

The thermogravimetry tests carried out here at three levels of high temperature first showed that the behavior of both alloys was seemingly deteriorated by comparison with Nb-free alloys of same compositions concerning Co or Ni, Cr and C earlier studied in the same conditions. Indeed, concerning the cobalt-based alloys, the Nb-free ternary versions of which were already not very oxidation-resistant, one noticed faster oxidation and very limited parabolic part of the mass gain kinetic. This led shortly to catastrophic oxidation, not really limited by the presence of external oxides the complexity and lack of quality of which were particularly great. This led to much thicker oxide scales (fast oxidation) but to less deep subsurface zones impoverished in chromium and in carbides than the nickel alloy. Indeed, when the cobalt alloy suffered general oxidation (oxidation of not only Cr but also the other metallic elements) instead selective oxidation of mainly chromium, the oxidation of the nickel alloy principally concerned chromium even if nickel oxide or spinel oxides involving Nb and Cr also formed. One finds again the same hierarchy as between the ternary Nb-free cobalt-based and the Nb-free nickel-based alloys. The presence of niobium induced an acceleration of oxidation in both cases, more sensible for the cobalt alloy than for the nickel one, but the morphology of NbC also influenced the global oxidation behavior, in a detrimental way. Thus, preliminarily aging the alloys for fragmenting the NbC interdendritic carbides to limit the outward Nb diffusion and reduce the detrimental effect of this element on the oxidation front is not a good idea: not only the high temperature mechanical properties may be lowered but the oxidation resistance too. Concerning the oxide spallation behavior the effect of niobium is rather limited, the main factor remaining the thickness of the external oxide scale. Indeed thin scales (i.e. when chromia is the main oxide present and the temperature low, 1000°C) better resist spallation at cooling while spallation appears when the oxide is thicker (chromia formed during 46h at higher temperatures, multi-constituted oxides). Inversely, when the oxides scales are thick enough to constitute veritable oxide shells spallation during cooling does not occur.

Concerning the chemical and microstructure changes due to high temperature oxidation in these Nb-containing alloys, the behavior of Nb was not expected. Although the selectively oxidized elements tends to present a local content decreasing when coming close to the oxidation front, an increase was noticed here instead. This phenomenon was reported in some recent works [19, 20] dealing with the high temperature oxidation of a commercial Nb-containing nickel-based superalloy, in which it was explained as be caused by uphill diffusion

resulting from negative niobium activity gradient in the chromium depletion zone appearing in the subsurface. Similar effect of the local decrease in chromium was found for carbon in the same alloy.

Despite that the alloys studied here were rather different from the 625 alloy and that the range of temperatures of interest was higher here, the same niobium uphill diffusion was observed. Concerning carbon, it seems that it has diffused towards the oxidation front to be oxidized and to leave the alloys as gaseous specie. This was demonstrated in earlier works [21, 22] for similar (but Nb-free) alloys for temperatures higher than 1000°C in atmospheric air. Back diffusion of carbon was reported only for temperatures equal to or lower than 1000°C, in the same articles [21, 22]. This oxidation-induced decrease in carbon activity in the subsurface is known as being responsible of the development of a carbide-free zone from the scale/alloy interface.

## CONCLUSION

As this can be expected the addition of niobium to form MC carbides of a new nature tends to be detrimental for the behavior of cast chromium-rich cobalt-based and nickel-based alloys in oxidation at high temperature, as this was verified in the present work in the [1000, 1200°C]-range. However the effect is not as strong as one may think, the main effect remaining the one of the base element (cobalt or nickel), even if it must be taken into account. The main problem with the NbC carbides is its fragmentation phenomenon and its deleterious effect on the mechanical properties, which shows the importance of metallurgical studies to try stabilizing more their geometry at elevated temperature for long times (e.g. by finding chemical adjustments to reduce the matrix-NbC interfacial energy). Concerning hot oxidation, increase in chromium content or subsurface Cr-enrichment by pack-cementation may be efficient solutions. To finish one can highlight that the presence of Nb with rather high content and with the form of carbides led to complex corrosion products interesting to study for describing mechanisms. Further work may be envisaged by carrying out oxidation over different durations or XRD-followed oxidation tests, for instance.

## References

1. M. J. Donachie, S. J. Donachie, *Superalloys: A Technical Guide (2<sup>nd</sup> Edition)*, Materials Park: ASM International, 2002.
2. B. Gorr, S. Burk, T. Depka, et al, *International Journal of Materials Research (formerly Z. Metallkd.)* **103**, 24 (2012).
3. C. Cui, D. Ping, Y. Gu, et al, *Materials Transactions* **47**, 2099 (2006).
4. B. Gorr, M. Azim, H.-J. Christ, et al, *Metallurgical and Materials Transactions A: Physical Metallurgy and Materials Science* **47**, 961 (2016).
5. P. Berthod, *Journal of Alloys and Compounds* **481**, 746 (2009).
6. P. Berthod, E. Conrath, *Materials Chemistry and Physics* **143**, 1139 (2014).
7. E. Conrath, P. Berthod, *International Journal of Materials Research (formerly Z. Metallkd.)* **105**, 717 (2014).
8. P. Berthod, E. Conrath, *Materials at High Temperature* **31**, 266 (2014).
9. P. Berthod, E. Conrath, *Materials and Design* **104**, 27 (2016).
10. P. Berthod, E. Conrath, *Journal of Materials Science and Technology Research* **1**, 7 (2014).
11. P. Berthod, *Advances in Materials Science and Engineering*, Article ID 4145369, <https://doi.org/10.1155/2017/4145369>.
12. P. Berthod, *Advanced Materials Letters* **8(8)**, 866 (2017).
13. C. T. Sims, *High Temperature Technology* **2**, 185 (1984).
14. M. C. Dropmann, D. Stover, H. P. Buchkremer, et al, *Advances in Powder Metallurgy and Particulate Materials* **8**, 213 (1992).
15. D. Young, *High Temperature Oxidation and Corrosion of Metals*, Amsterdam: Elsevier Corrosion Series, 2008.
16. E. Conrath, P. Berthod, *Corrosion Engineering, Science and Technology* **49(1)**, 45 (2014).
17. P. Berthod, E. Conrath, *Canadian Metallurgical Quarterly*, **55(4)**, 409 (2016).
18. E. Conrath, P. Berthod, *The Open Materials Science Journal* **10**, 89 (2016).
19. A. Chyrkin, P. Huczkowski, V. Shemet, L. Singheiser, W. J. Quadackers, *Oxidation of Metals* **75**, 143 (2011).
20. L. Garcia-Fresnillo, A. Chyrkin, C. Böhme, J. Barnikel, F. Schmitz, W. J. Quadackers, *Journal of Materials Science*, **49(17)**, 6127 (2014).
21. P. Berthod, S. Michon, J. Di Martino, S. Mathieu, S. Noël, R. Podor, C. Rapin, *Calphad* **27**, 279 (2003).
22. P. Berthod, C. Vébert, L. Aranda, R. Podor, C. Rapin, *Oxidation of Metals* **63(1/2)**, 57 (2005).

**TABLE 1.** Compositions of CoNb and NiNb elaborated alloys.

wt.%	Co	Ni	Cr	C	Nb
CoNb	Bal.	/	25	0.5	3.9
NiNb	/	Bal.	25	0.5	3.9

**TABLE 2.** Values of the linear constant  $k_l$ , of the parabolic constant  $k_p$  and of the constant chromia volatilization constant  $k_v$ , the two later ones being derived from the  $m \times dm/dt = f(m)$  plots.

Alloys	1000°C	1100°C	1200°C
	$k_p$	$k_p$	$k_p$
	$\times 10^{-12}$ $g^2.cm^{-4}.s^{-1}$	$\times 10^{-12}$ $g^2.cm^{-4}.s^{-1}$	$\times 10^{-12}$ $g^2.cm^{-4}.s^{-1}$
NiNb	2.4	18	90
NiNbR	7.2	20	105
CoNb	Non-parabolic curve	Non-parabolic curve	6960
CoNbR	Non-parabolic curve	4050	7930

**TABLE 3.** Comparison of kinetic constants obtained for Nb-containing alloys in this study and those obtained for the ternary alloys in recent works.

Alloys	1100°C	1200°C
	$k_p$	$k_p$
	$\times 10^{12}$ $g^2.cm^{-4}.s^{-1}$	$\times 10^{12}$ $g^2.cm^{-4}.s^{-1}$
NiNb	18	90
Ni-25Cr-0.5C [9]	5.5	/
CoNb	Non-parabolic curve	6960
Co-25Cr-0.5C [17, 16]	15	59

**TABLE 4.** Spallation's start temperatures of oxide layers and lost masses during the cooling of thermogravimetric samples of all alloys at all test temperatures.

Alloys	1000°C		1100°C		1200°C	
	Spallation's start temperature	Lost mass during the cooling	Spallation's start temperature	Lost mass during the cooling	Spallation's start temperature	Lost mass during the cooling
	°C	$g/cm^2$	°C	$g/cm^2$	°C	$g/cm^2$
NiNb	No spallation		$\approx 740$	$6.8 \times 10^{-3}$	$\approx 860$	$1.7 \times 10^{-2}$
NiNbR	No spallation		$\approx 750$	$7.4 \times 10^{-3}$	$\approx 870$	$1.7 \times 10^{-2}$
CoNb	$\approx 320$	$1.0 \times 10^{-2}$	No spallation		No spallation	
CoNbR	$\approx 300$	$9.5 \times 10^{-3}$	No spallation		No spallation	

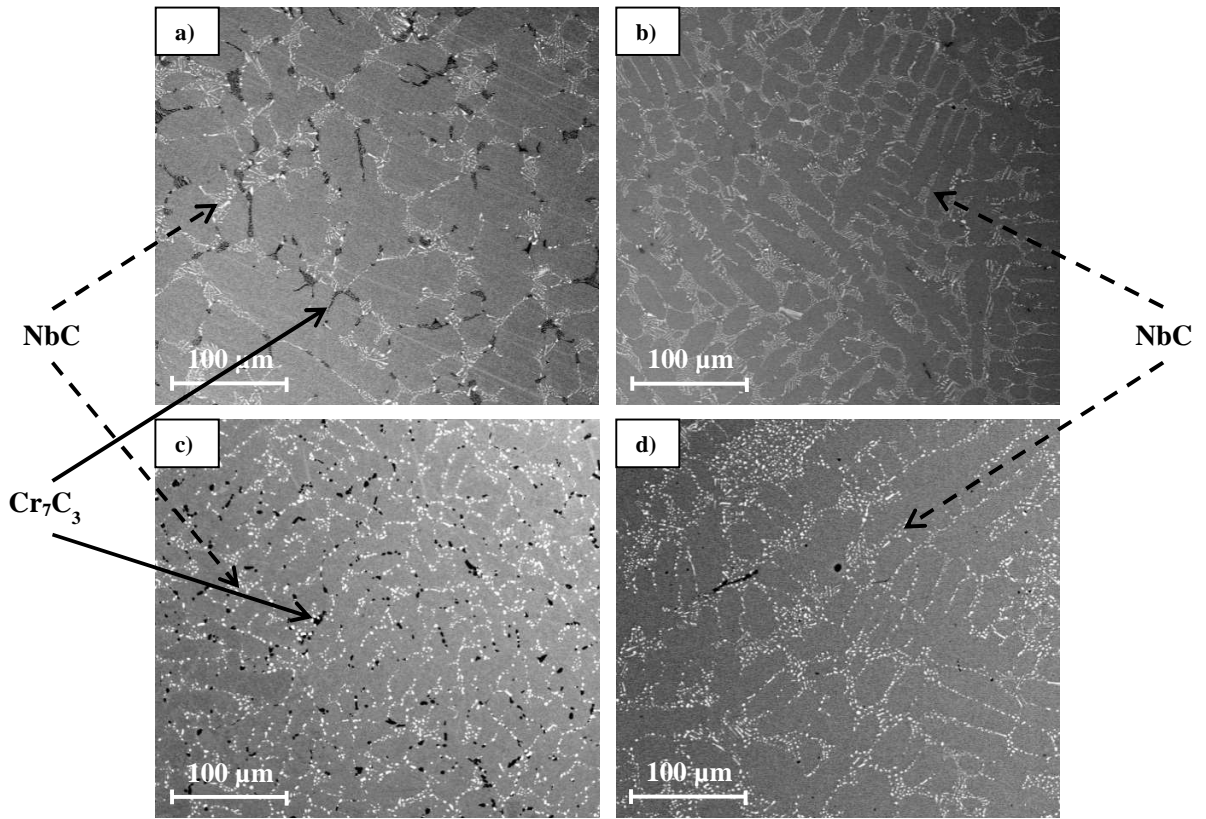


**FIGURE 1.** SEM images in BSE mode of the alloys: a) NiNb, b) CoNb, c) NiNbR and d) CoNbR.

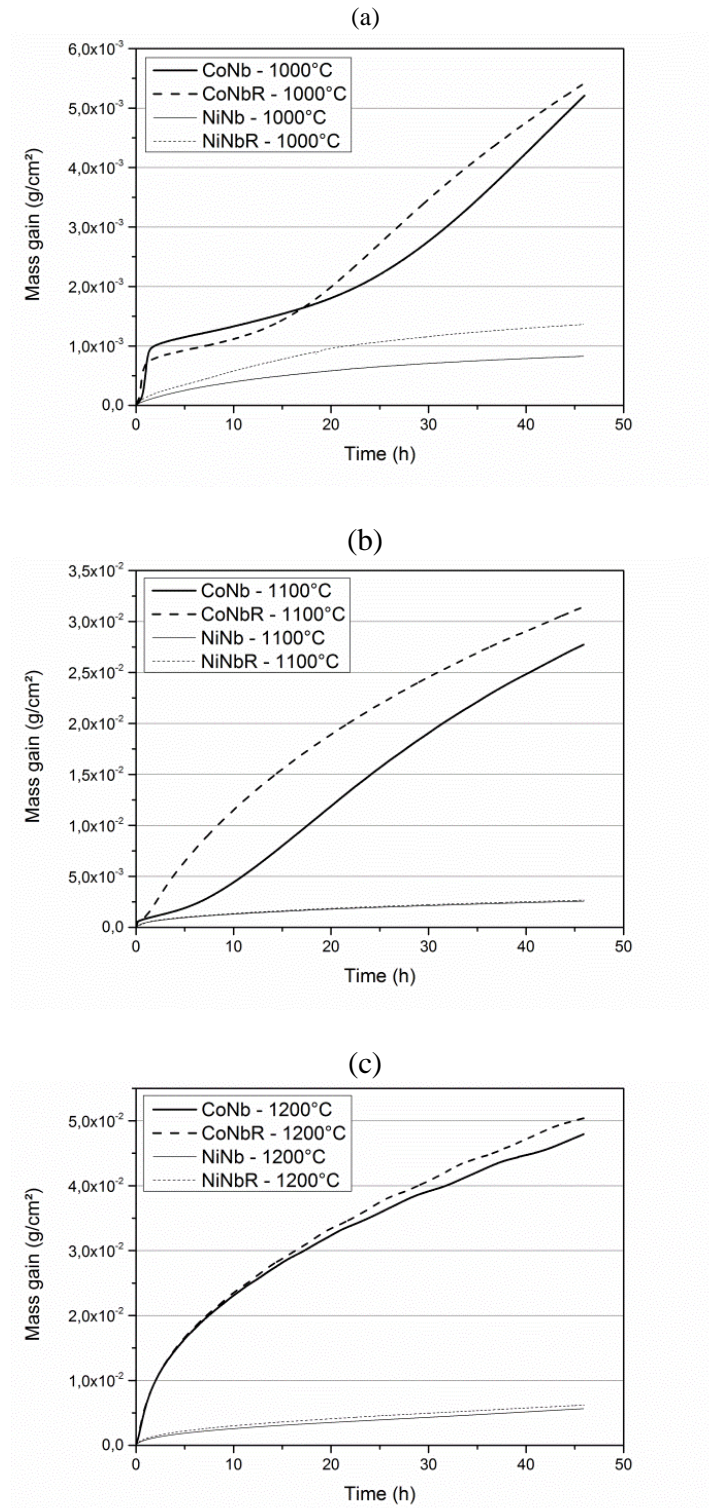


**FIGURE 2.** Mass gain versus time plotted of NiNb, NiNbR, CoNb and CoNbR alloys at 1000°C (a), 1100°C (b) and 1200°C (c) during 46h.

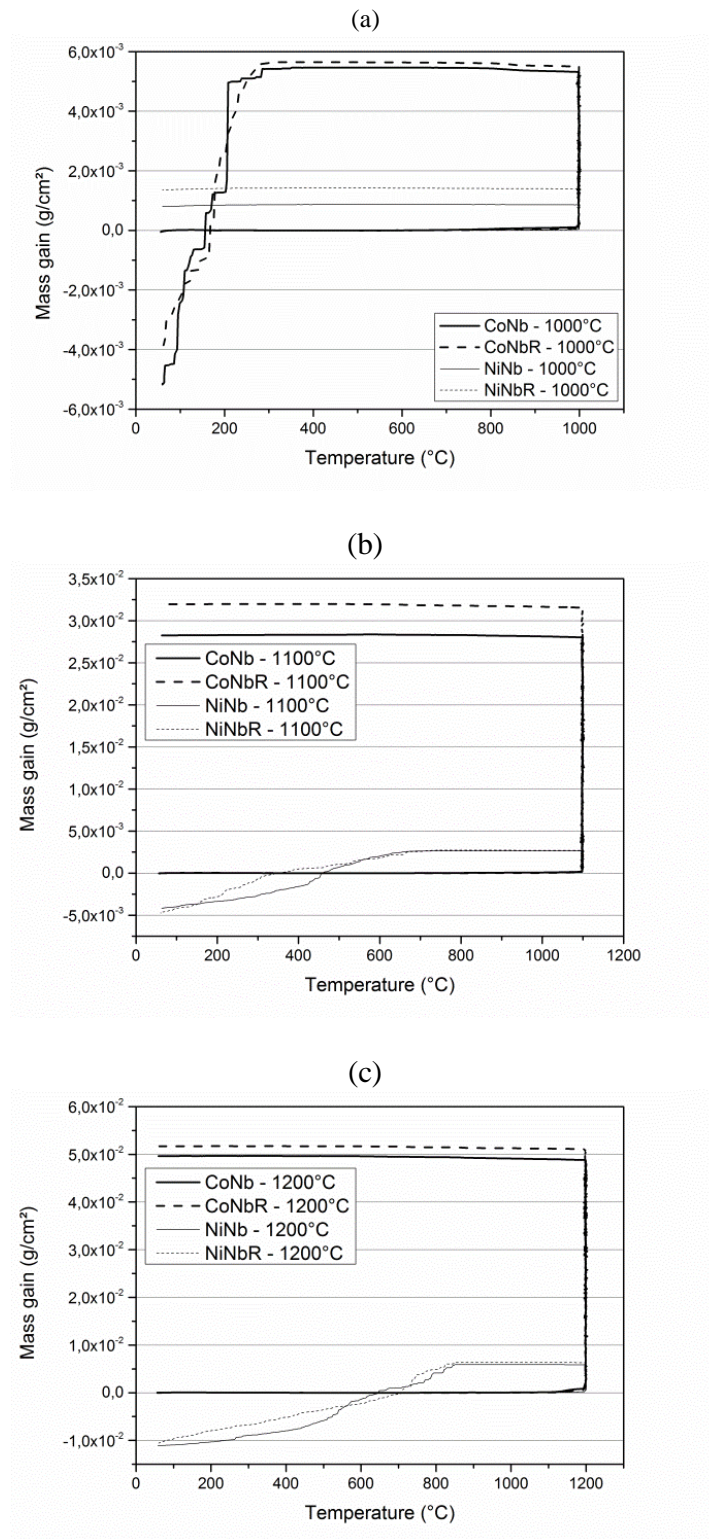


**FIGURE 3.** Mass gain curves versus temperature of thermogravimetric tests for NiNb, NiNbR, CoNb and CoNbR alloys at 1000°C, 1100°C and 1200°C during 46h.

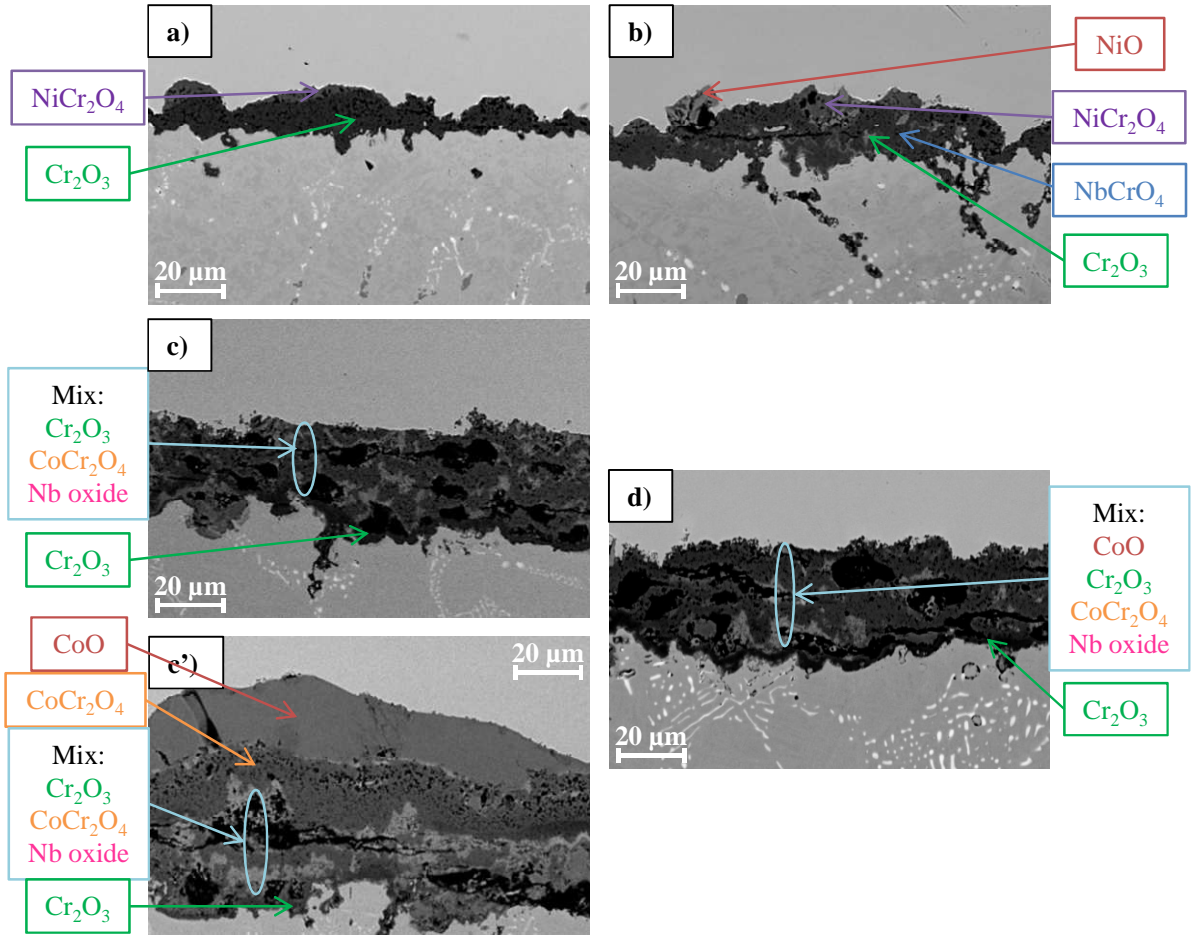


**FIGURE 4.** SEM/BSE images of oxide layers after the oxidation at 1000°C during 46h for a) NiNb alloy, b) NiNbR alloy, c) and c') CoNb alloy and d) CoNbR alloy.

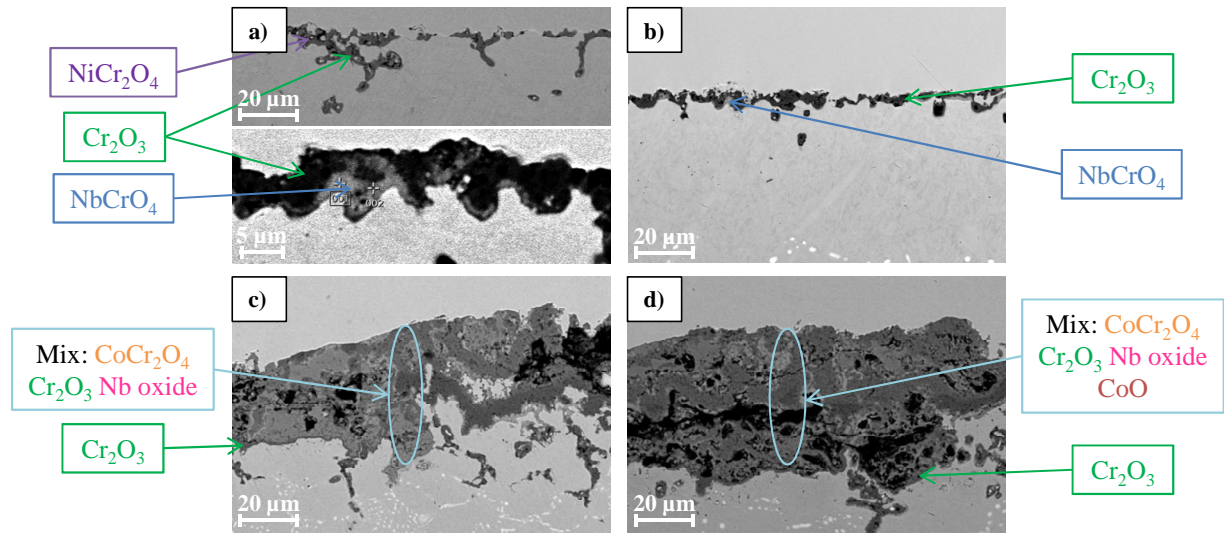


**FIGURE 5.** SEM/BSE images of oxide layers after the oxidation at 1100°C during 46h for a) NiNb alloy, b) NiNbR alloy, c) CoNb alloy and d) CoNbR alloy.

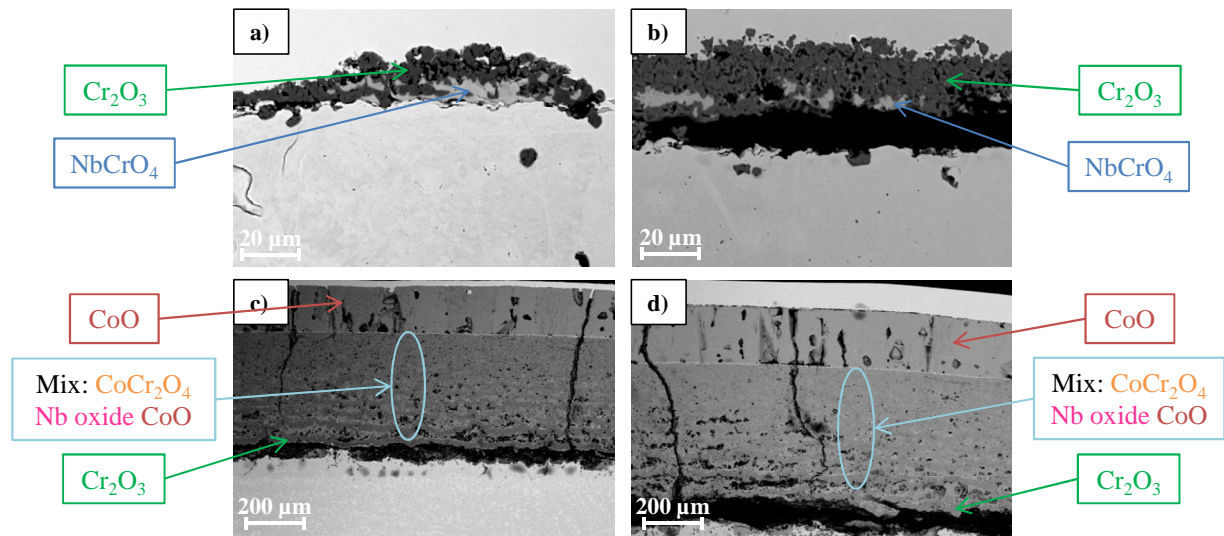


**FIGURE 6.** SEM/BSE images of oxide layers after the oxidation at 1200°C during 46h for a) NiNb alloy, b) NiNbR alloy, c) CoNb alloy and d) CoNbR alloy.

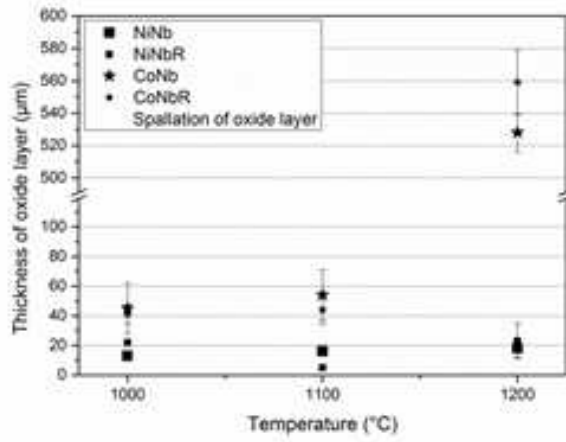


**FIGURE 7.** Thicknesses of oxide layers of both alloys in as-cast and aged states after the oxidation at 1000°C, 1100°C and 1200°C.

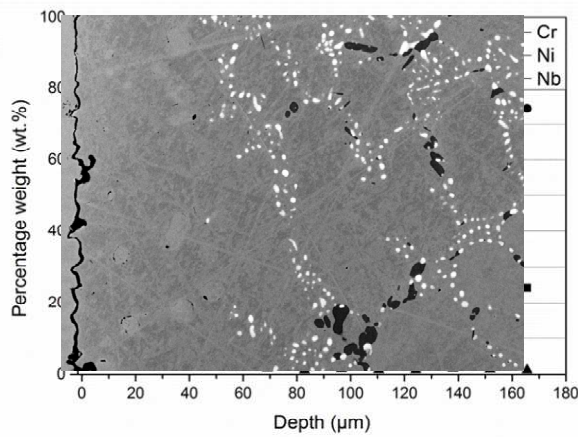


**FIGURE 8.** SEM/BSE image and concentration profiles of Cr, Ni and Ni at the sub-surface of oxidized NiNbR alloy at 1200°C.

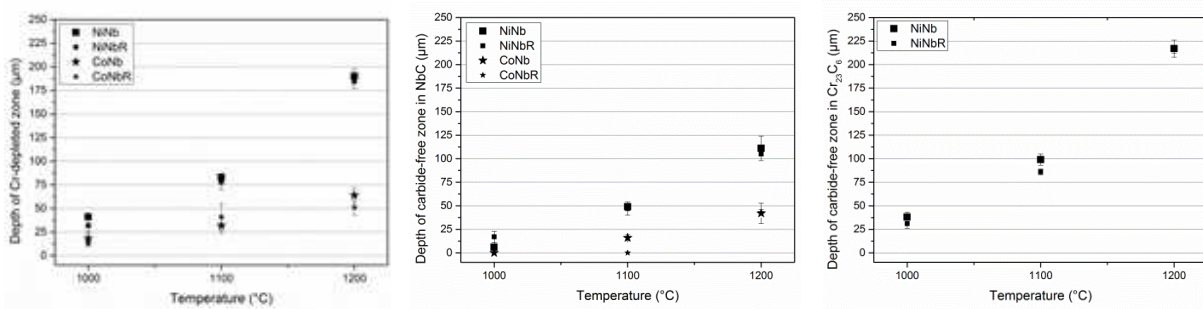


**FIGURE 9.** Depths of Cr-depleted and carbides-free zones created by oxidation at sub-surface of samples.